Quantum thermalization and the route to ergodicity

Amichay Vardi [1,2,*] and Doron Cohen [3,†]
[1]Department of Chemistry, Ben-Gurion University of the Negev, Beer-Sheva 84105, Israel
[2]ITAMP, Harvard-Smithsonian Center for Astrophysics, Cambridge, Massachusetts 02138, USA
[3]Department of Physics, Ben-Gurion University of the Negev, Beer-Sheva 84105, Israel

(Received 29 July 2025; accepted 14 November 2025; published 15 December 2025; corrected 26 January 2026)

We consider a minimal model for quantum thermalization of coupled chaotic subsystems. The route toward ergodicity is explored as a function of the coupling strength. The results are contrasted with the predictions of standard random matrix theory and the eigenstates thermalization hypothesis. We highlight a coupling regime of disparity between the spectral statistics that indicates chaos and ergodicity measures that indicate lack of eigenstate thermalization. The analysis involves a revision of the energy-shell concept, in a way that is consistent but independent of the semiclassical perspective.

DOI: 10.1103/7355-1nlj

I. INTRODUCTION

Random matrix theory (RMT), and specifically the theory of Wigner banded random matrices (WBRM) [1,2], has been proposed as a framework to describe ergodization and thermalization. Consider the quantum thermalization between coupled subsystems of a bipartite disordered system, where each subsystem by itself is generically chaotic. The Hamiltonian is $H = H_0 + \lambda V$, where the intersystem interaction λV mixes the eigenstates of the uncoupled subsystems.

It has been previously realized that generic perturbations of a quantized chaotic system (QCS) can be modeled by WBRM [3–9]. It follows that for relatively weak coupling the mixing of the levels is described by the Wigner Lorentzian, while for strong coupling the line shape becomes nonperturbative. Namely, for WBRM, it is a semicircle line shape, while for a QCS it is a semiclassical line shape that reflects the underlying phase-space geometry. The latter is implied by the association of chaotic eigenstates with microcanonical distributions in Berry's conjecture and the eigenstate thermalization hypothesis (ETH) [10–16].

Later studies have considered the route to ergodicity and thermalization of large arrays, with special emphasis on one-dimensional (1D) chains [17–20], utilizing both spectral and ETH measures [21,22]. In such studies, H_0 is integrable, while λV spoils the integrability. Here, we consider a more appropriate modeling of thermalization, closer in spirit to the traditional thermodynamic concept, where Boltzmann's "molecular chaos" applies equally well to the constituent thermalizing subsystems. Accordingly, we consider below a model for thermalization, where λV is the coupling between the quantized *chaotic* subsystems. Each subsystem is chaotic by itself, while the coupling allows exchange of particles and energy. This configuration may be thought of as "vintage thermalization" because it reflects the traditional 19th-century reasoning of thermodynamics. Similar agenda has been presented in Ref. [23].

As shown below, the application of WBRM theory to vintage thermalization is rather subtle. For illustration, we consider a bipartite Bose-Hubbard model (BHM) [24–31]. The eigenstates of the disconnected subsystems $H_0|x,n\rangle = \varepsilon_{x,n}|x,n\rangle$ are direct products of subsystem eigenstates with well-defined integer subsystem occupations, indexed by two good quantum numbers: the occupation difference x and the index n of the state within the factorized spectrum (for a given x). These are plotted in Fig. 1, where each point represents an unperturbed eigenstate. The coupling $\langle x,n|V|x',n'\rangle$ connects only states with $|x-x'|=1$. This two-dimensional (2D) geometry of the basis for the BHM is very different from the 1D geometry of the WBRM (left panel of Fig. 1), with substantial implications on the route to ergodicity.

Outline

We introduce the model and basic definitions in Secs. II and III. Critical discussion of the energy-shell concept is provided in Sec. IV. Identification of chaos and ergodicity is explained in Secs. V and VI. Then, we explore the route toward ergodicity for the BHM in Sec. VII, and contrast it with the WBRM. Auxiliary issues related to ergodicity measures and regime boundaries are discussed in Secs. VIII and IX. Finally, discussion and summary are provided in Sec. X. Appendix A provides a terse summary of the WBRM regimes, while Appendix B presents extra numerical demonstration for the irrelevance of subsystem geometry.

II. THE BHM

Consider the bipartite BHM for N particles in $M = M_A + M_B$ sites, where M_α is the number of sites in subsystem

*Contact author: avardi@bgu.ac.il
†Contact author: dcohen@bgu.ac.il

Published by the American Physical Society under the terms of the Creative Commons Attribution 4.0 International license. Further distribution of this work must maintain attribution to the author(s) and the published article's title, journal citation, and DOI.

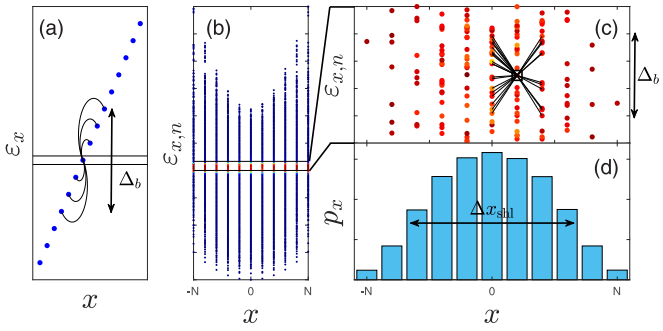


FIG. 1. The unperturbed basis. The unperturbed energies ε_x and $\varepsilon_{x,n}$ for the WBRM [panel (a)] and for the BHM [panels (b) and (c)], respectively. The bandwidth Δ_b is the maximal range in energy that can be reached by a single transition from an initial state. Possible first-order transitions are indicated. The width of the energy shell $\Delta x_{\rm shl}$ is defined via the microcanonical distribution p_x [panel (d)]. It is not sensitive to λ for the BHM, and has a well-defined finite value in the limit of zero coupling. In contrast, the WBRM model can be regarded as a singular limit that features $\Delta x_{\rm shl} \propto \lambda$.

$\alpha = A, B$. The Hamiltonian is

$$H = \sum_{\alpha=A,B} H_\alpha + \lambda V, \tag{1}$$

where the subsystem Hamiltonians are

$$H_\alpha = \sum_i \varepsilon_{\alpha,i}\hat{n}_{\alpha,i} + \frac{U}{2}\sum_i \hat{n}_{\alpha,i}(\hat{n}_{\alpha,i}-1) - K\left(\sum_{\langle i,j\rangle} \hat{a}^\dagger_{\alpha,i}\hat{a}_{\alpha,j} + \text{H.c.}\right) \tag{2}$$

and the intersystem coupling is

$$V = \hat{a}^\dagger_{A,1}\hat{a}_{B,1} + \hat{a}^\dagger_{A,M_A}\hat{a}_{B,M_B} + \text{H.c.}$$

In the above, the boson operator $\hat{a}_{\alpha,i}$ annihilates a particle in the ith site of the α subsystem with population $\hat{n}_{\alpha,i} = \hat{a}^\dagger_{\alpha,i}\hat{a}_{\alpha,i}$, the intrasystem hopping frequency is K, and $\langle i, j\rangle$ denotes nearest-neighbor pairs. The coupling strength is U, and the weak on-site random potential $\varepsilon_{\alpha,i}$ breaks parity. In the numerical demonstrations, we have $M_A = M_B = 4$, $N = 10$, and $|\varepsilon_{\alpha,i}| < 0.05$, while $K = 1$ and $U = 1$.

The Hilbert-space dimension of the BHM is

$$D_M(N) = \frac{(N+M-1)!}{N!(M-1)!} = \sum_{x=-N}^{N} D_x, \tag{3}$$

where $D_x = D_{M_A}(\frac{N+x}{2}) \times D_{M_B}(\frac{N-x}{2})$ is the dimension of the x sector of the spectrum (i.e., the number of states in each column of the diagram in Fig. 1) and $x = -N, -N+2, \ldots, N-2, N$. In the absence of intersystem coupling ($\lambda = 0$), the eigenenergies of the unperturbed Hamiltonian $H_0 = H_A + H_B$ are $\varepsilon_{x,n}$, where the running index $n = 1, \ldots, D_x$ labels the x-sorted unperturbed energies.

III. EIGENSTATES OF THE COUPLED SUBSYSTEMS

Once the coupling λ is turned on, the subsystems can exchange particles, and the coordinate x is no longer a good quantum number. Accordingly, we use a running index $\nu = 1, \ldots, D_M(N)$ to label the many-body eigenstates and the respective eigenenergies E_ν. In the presentated results below, these energies are scaled as $E := (E - E_{\rm min})/(E_{\rm max} - E_{\rm min})$, where $E_{\rm min}$ and $E_{\rm max}$ are the ground and top energies.

Each exact eigenstate features a probability distribution over the unperturbed states, namely,

$$p^{(\nu)}_{x,n} = |\langle x, n|E_\nu\rangle|^2. \tag{4}$$

The associated population imbalance and energy distributions are

$$p^{(\nu)}_x = \sum_n p^{(\nu)}_{x,n}, \tag{5}$$

$$p^{(\nu)}(\varepsilon) = \sum_{x,n} p^{(\nu)}_{x,n}\,\delta(\varepsilon - \varepsilon_{x,n}). \tag{6}$$

Using the above probability distributions, we define the following measures for the eigenstates, characterizing their spreading over the unperturbed basis:

$$P_\nu = \max_{x,\nu}\left\{p^{(\nu)}_{x,n}\right\} = \text{peak probability}, \tag{7}$$

$$\mathcal{M}_\nu = \left[\sum_{x,n}\left|p^{(\nu)}_{x,n}\right|^2\right]^{-1} = \text{participation number}, \tag{8}$$

$$\Delta x_\nu = \text{dispersion of } x \text{ via Eq. (5)}, \tag{9}$$

$$\Delta\varepsilon_\nu = \text{dispersion of } \varepsilon \text{ via Eq. (6)}. \tag{10}$$

The peak probability indicates whether the exact eigenstate $|E_\nu\rangle$ is a first-order perturbed eigenstate $|x, n\rangle$ of the uncoupled system. The participation number estimates the number of unperturbed eigenstates that contribute to the exact eigenstate. The dispersions quantify the spread in x and in ε. It should be noted that while the full energy dispersion of an exact eigenstate is identically zero, $\Delta\varepsilon_\nu$ is the dispersion over the *unperturbed* energies, i.e., $\Delta\varepsilon_\nu = [\langle H_0^2\rangle_\nu - \langle H_0\rangle_\nu^2]^{1/2}$.

IV. THE ENERGY SHELL

Semiclassically, a microcanonical distribution occupies an energy shell of thickness δE in phase space. In the classical context, the "energy surface" limit, $\delta E \to 0$, is well defined. Quantum mechanically, the thickness δE should be large with respect to the mean level spacing but small with respect to the energy scale on which this spacing varies; i.e., the shell width should be "classically small but quantum mechanically large."

It is practically useful to project the shell either over x or over ε to obtain the shell probability distributions p_x and $p(\varepsilon)$. This means that $p_x \equiv \overline{p^{(\nu)}_x}$ and $p(\varepsilon) \equiv \overline{p^{(\nu)}(\varepsilon)}$ are obtained by, respectively, averaging $p^{(\nu)}_x$ and $p^{(\nu)}(\varepsilon)$ over eigenstates ν that belong to the δE energy window, i.e., $|E_\nu - E| < \delta E/2$. We define the dispersion $\Delta x_{\rm shl}$ as the second moment of the distribution p_x, as illustrated in Fig. 1. Similarly, we extract the dispersion $\Delta\varepsilon_{\rm shl}$ from the unperturbed energy distribution $p(\varepsilon)$.

In Fig. 2, we plot the dependence of $\Delta x_{\rm shl}$ and $\Delta\varepsilon_{\rm shl}$ on the arbitrary chosen window δE and the coupling strength λ. When δE is large with respect to the level spacing, the shape

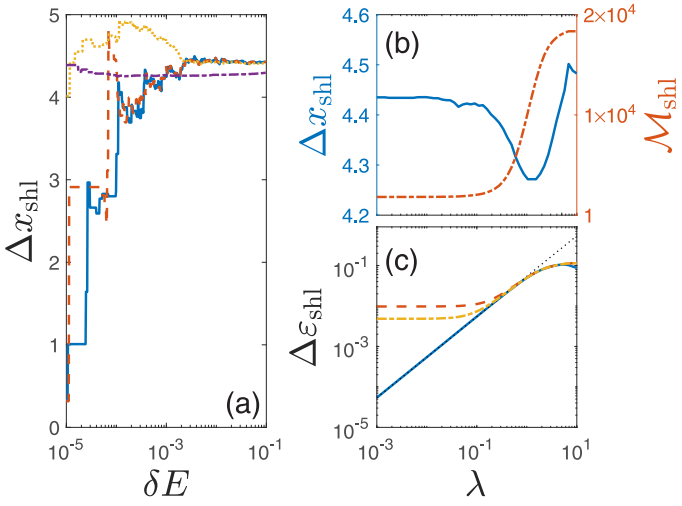


FIG. 2. The width of the energy shell. (a) The width $\Delta x_{\rm shl}$ vs the width δE of the arbitrary energy window about $E = 0.4167$ for $\lambda = 10^{-3}$ (solid blue line), 10^{-2} (dashed red), 10^{-1} (dotted orange), and 1.0 (dash-dotted purple). The width of the energy shell is well defined (assuming quantum mechanically large but classically small δE) and the dependence of the obtained shell width on the coupling strength λ is weak. (b), (c) The dependence of $\Delta x_{\rm shl}$, $\mathcal{M}_{\rm shl}$, and $\Delta\varepsilon_{\rm shl}$ on the coupling λ. In the latter case, one observes a residual value for small λ, corresponding to the arbitrary δE (dashed line is for $\delta E = 0.0333$, whereas dash-dotted line is for $\delta E = 0.0166$). This numerical artifact can be eliminated by looking on $\overline{\Delta\varepsilon_\nu}$ (solid line), even if the eigenstates are nonergodic. The dotted line is a guide to the eye, corresponding to linear $\Delta\varepsilon_{\rm shl}(\lambda)$ dependence.

of $p(x)$ becomes independent of δE and only very weakly dependent on λ. Thus, the dispersion $\Delta x_{\rm shl}$ is well defined.

In contrast, the energy dispersion $\Delta\varepsilon_{\rm shl}$ approaches the arbitrary window width δE at small λ. This numerical artifact indicates that δE is still too large. The dispersion $\Delta\varepsilon_{\rm shl}$ is the convolution of the individual widths $\Delta\varepsilon_\nu$ with the arbitrary δE. Physically meaningful result is obtained provided the contribution of δE is negligible. It turns out that this numerical limitation can be avoided, because for classically small λ we get

$$\Delta\varepsilon_{\rm shl} = \overline{\Delta\varepsilon_\nu} = \lambda\sqrt{[V^2]_{\varepsilon,\varepsilon} - [V]^2_{\varepsilon,\varepsilon}}. \tag{11}$$

This holds even if the eigenstates are nonergodic, as further discussed in the following subsections with consequences that are highlighted in Sec. IX. Figure 2(c) demonstrates the validity of this statement, and the implied linear dependence of $\Delta\varepsilon_{\rm shl}$ on λ.

A. Width of the energy shell

Denoting unperturbed and exact eigenstates as $|\varepsilon\rangle$ and $|E\rangle$, respectively, the local density of states (LDOS) and the inverse-LDOS (the lineshape of the eigenstates) are defined, respectively, as follows:

$$P^{(\varepsilon)}(E) = |\langle E|\varepsilon\rangle|^2, \tag{12}$$

$$p^{(E)}(\varepsilon) = |\langle\varepsilon|E\rangle|^2. \tag{13}$$

What we call $\Delta\varepsilon_{\rm shl}$ is the ε width of $p^{(E)}(\varepsilon)$, while Δ_E is defined as the E width of $P^{(\varepsilon)}(E)$. Let us first clarify these definitions in a purely classical context. Assume that $H(X,P) = H_0 + \lambda V$. Consider a microcanonical distribution $H_0(X,P) = \varepsilon$ and define $E = H(X,P)$. We have the trivial identity

$$\Delta_E^2 = \lambda^2\big[\langle V(X,P)^2\rangle_\varepsilon - \langle V(X,P)\rangle_\varepsilon^2\big], \tag{14}$$

where the ε subscript indicates an H_0-microcanonical phase-space average. This result implies strict linear dependence $\Delta_E \propto \lambda$. The dual statement for the inverse-LDOS is as follows. Consider a microcanonical distribution $H(X,P) = E$ and define $\varepsilon = H_0(X,P)$. We have the trivial identity

$$\Delta\varepsilon^2 = \lambda^2\big[\langle V(X,P)^2\rangle_E - \langle V(X,P)\rangle_E^2\big], \tag{15}$$

where the E subscript indicates an H-microcanonical phase-space average. Here, there is an implicit λ dependence of the latter. But if the difference between the surfaces $H(X,P) = E$ and the surfaces $H_0(X,P) = \varepsilon$ is small, the H microcanonical average can be calculated with an unperturbed surface of H_0, and the same result will be obtained, approximately, provided λ is classically small enough.

B. Second moment energy spreading

Here, we provide the proof that the second moment of the energy spreading has a robust linear dependence of λ, provided the perturbation is classically small, irrespective of quantum ergodicity. The proof is merely a translation of the classical statement Eq. (15) into quantum language. We assume that $H = H_0 + \lambda V$. Let $|\varepsilon\rangle$ be the eigenvalues of H_0, and let $|E\rangle$ be a chosen eigenstate of H. Then, it follows that

$$\Delta\varepsilon = \lambda\sqrt{\langle E|V^2|E\rangle\langle E|V|E\rangle^2}, \tag{16}$$

$$\approx \lambda\sqrt{[V^2]_{\varepsilon,\varepsilon} - [V]^2_{\varepsilon,\varepsilon}} \equiv \Delta_E \tag{17}$$

with $\varepsilon = E$. This result, which we further explain below, is independent of whether the eigenstate is quantum ergodic or not. The validity of this observation can be optionally verified by direct calculation of the second moment spreading for the nonergodic perturbative eigenstates of Eq. (20).

Let us elaborate on the two steps in Eq. (16). The first equality is based on a trivial identity that holds for the $k = 1, 2$ moments (and cannot be extended to higher moments due to operator-ordering issue):

$$\begin{aligned}\langle\varepsilon^k\rangle &= \sum_\varepsilon |\langle\varepsilon|E\rangle|^2\varepsilon^k = \big\langle E|H_0^k|E\big\rangle \\ &= \langle E|(H-\lambda V)^k|E\rangle \\ &= \begin{cases} E - \lambda\langle E|V|E\rangle & |\text{for } k=1 \\ E^2 - 2\lambda E\langle E|V|E\rangle + \langle E|V^2|E\rangle & |\text{for } k=2 \end{cases}.\end{aligned}$$

The second equality in Eq. (16) holds for a *classically small* λ, because the matrix elements of any generic operator between perturbed eigenstates are approximately equal to the matrix elements between the unperturbed eigenstates, namely,

$$\langle E|A|E\rangle \approx \langle\varepsilon|A|\varepsilon\rangle \equiv A_{\varepsilon,\varepsilon} \quad \text{with} \quad \varepsilon \approx E. \tag{18}$$

This approximation is based on the observation that $\langle\psi|A|\psi\rangle = \text{trace}[A\rho]$ with $\rho = |\Psi\rangle\langle\Psi|$ can be written as a

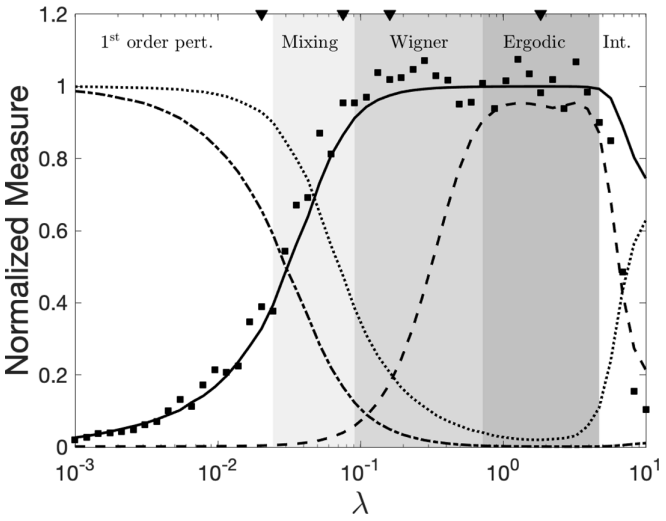


FIG. 3. Chaos and ergodicity measures. Misc measures are calculated for the energy shell $0.4 < E < 0.4333$ as a function of the coupling strength λ, and normalized per the expected GOE values. The spectral measure for chaos $\tilde{r}$ (square markers) is correlated with $\overline{\Delta x_\nu}/\Delta x_{\rm shl}$ (solid line). The ETH measure $\sigma_x/\Delta x_{\rm shl}$ (dotted line) is an insufficient measure for ergodization. The measure $\overline{\mathcal{M}_\nu}/(\mathcal{M}_{\rm shl}/3)$ (dashed line) is an effective measure for the actual identification of the ergodic regime. We also plot the mean peak probability $\overline{P_\nu}$ (dash-dotted line), which is used to identify the first-order perturbative regime (arbitrarily defined as $\overline{P_\nu} > 0.6$). Inverted triangles mark the coupling strengths for the states presented in Fig. 4.

phase-space integral over Wigner functions. If the microcanonical energy surface that supports ρ is not related to the phase-space contours of A, the trace overlap is rather robust. A small perturbation to ψ will not affect systematically the result (i.e., disregarding quantum fluctuations).

V. DISTINGUISHING ERGODICITY FROM CHAOS

It is a common misconception to identify "quantum chaos" with "quantum ergodicity." Quantum chaos is identified by the spectral statistics. In Fig. 3, we display a rescaled version of a common measure for level repulsion, namely, the mean ratio of consecutive level spacings [32]:

$$\tilde{r} \equiv \frac{\langle r\rangle - r_{\rm Poisson}}{r_{\rm GOE} - r_{\rm Poisson}}. \tag{19}$$

The value $\langle r\rangle = r_{\rm Poisson} = 0.38\,629$ $(\tilde{r}=0)$ characterizes spectra that consist of uncorrelated levels. This applies to integrable systems but also to the uncoupled chaotic systems of our model. The value $\langle r\rangle = r_{\rm GOE} = 0.53590$ $(\tilde{r}=1)$ holds for spectra of fully chaotic systems with Wigner-Dyson level spacing statistics.

The proper measure for the quantum ergodicity of the eigenstates is the mean participation number $\overline{\mathcal{M}_\nu}/\mathcal{M}_{\rm shl}$ (dashed line in Fig. 3). The $\mathcal{M}_\nu$ are calculated for the individual eigenstates, while $\mathcal{M}_{\rm shl}$ is calculated from the $p_{x,n}$ of the energy shell. For GOE statistics, a value of $\overline{\mathcal{M}_\nu}/\mathcal{M}_{\rm shl} \approx 1/3$ indicates the ergodicity of the eigenstates. The 1/3 factor emerges because the $p^{(\nu)}_{x,n}$ probabilities are not uniformly spread over the energy shell but statistically fluctuate.

Comparing the two measures, we note that the ergodic regime in Fig. 3 is much smaller than the chaotic regime indicated by spectral statistics. For a substantial λ range, the system is chaotic, yet its eigenstates are not ergodic. Similar discrepancies between chaos and ergodization measures have been previously observed without further exploration in [33–36].

VI. THE ETH ERGODICITY MEASURES

The ETH predicts that for ergodic eigenstates $|E_\nu\rangle$ the expectation value of any local observable, such as $\langle x\rangle_\nu$, will exhibit low state-to-state fluctuations, with dispersion $\sigma_x \propto 1/\sqrt{\mathcal{M}}$. The mere decrease of state-to-state fluctuations, however, is not a sufficient indication for ergodicity, as clearly demonstrated by comparing the earlier (weak coupling) drop of σ_x with the later (stronger coupling) rise of $\overline{\mathcal{M}_\nu}$ in Fig. 3.

VII. CONTRAST WITH WIGNER THEORY

Referring to the 2D energy landscape of the BHM (see Fig. 1), the width $\Delta x_{\rm shl}$ is finite, with negligible dependence on λ (see Fig. 2). This should be contrasted with the WBRM paradigm, where the horizontal and vertical dimensions are degenerate. Namely, $\Delta x_{\rm shl} = \Delta\varepsilon_{\rm shl}/\Delta_0$, where Δ_0 is the mean level spacing. Thus, in the WBRM model, x can be viewed as a dimensionless energy coordinate. This observation leads to the understanding that the mathematical-oriented WBRM model is an oversimplification. The actual route toward thermalization in a realistic physical system like the BHM is more complicated and nonuniversal.

VIII. THE ROUTE TO ERGODICITY

We identify five distinct physical regimes in the intricate progression of the BHM toward ergodicity, as the coupling strength λ increases. These are marked by the shaded regions in Fig. 3, with a representative eigenstate for each in Fig. 4. For the general discussion, we note that the relevant model parameters are the mean level spacing Δ_0, the bandwidth Δ_b, and the typical value $\bar{V}$ of the in-band matrix elements. It is useful to define dimensionless bandwidth $b = \Delta_E/\Delta_0$ and dimensionless coupling $\tilde{\lambda} := \lambda\bar{V}/\Delta_0$.

A. The perturbative regime

For very small values of λ, the peak probability P_ν is of order unity, and the $|E_\nu\rangle$ eigenstates can be described by first-order perturbation theory, which implies

$$p^{(\nu)}_{x,n} = \left|\frac{\langle x,n|\lambda V|x_0,n_0\rangle}{\varepsilon_{x,n} - \varepsilon_{x_0,n_0}}\right|^2, \quad (x,n) \neq (x_0,n_0), \tag{20}$$

where (x_0, n_0) indicates the unperturbed eigenstate. This approximation holds as long as $\tilde{\lambda} < 1$. It has been argued in Ref. [15] that Eq. (20) holds for the *tails* of the coarse-grained $p^{(\nu)}_{x,n}$ for larger values of λ, as long as quantum ergodicity is not yet attained. The validity of this claim for the BHM is

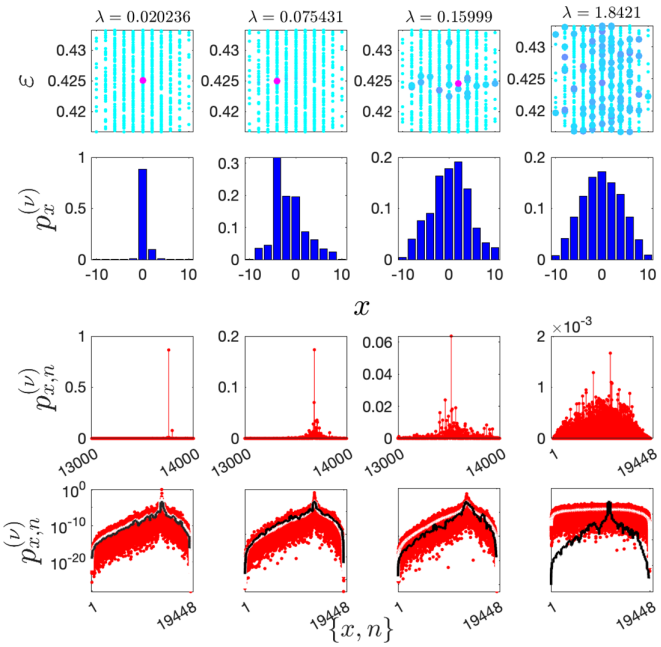


FIG. 4. Representative eigenstates. *Upper row*: Images of $p^{(\nu)}_{x,n}$ for a representative eigenstate with $E \approx 0.4167$. Each panel is for a different coupling corresponding (from left to right) to the perturbative, mixing, Wigner, and ergodic regimes. *Second row*: The resulting imbalance distribution $p^{(\nu)}_x$. *Third row*: The $p^{(\nu)}_{x,n}$ probabilities are plotted vs (x, n), arranged in order of ascending unperturbed energy. *Bottom row*: The same $p^{(\nu)}_{x,n}$ probabilities are compared on a log scale to the coarse-grained first-order perturbation profiles (solid lines). White lines are coarse-graining of $p^{(\nu)}_{x,n}$.

demonstrated with striking accuracy in the lower panels of Fig. 4.

B. The mixing regime

As λ is increased nearby levels are mixed, leading to level repulsion reflected by the spectral measure r. At this stage, the eigenstates spread in the "horizontal" x direction of the (x, ε) energy shell, yet remain localized in the "vertical" ε direction. A rough estimate for this horizontal mixing is provided by the standard Anderson model, predicting a localization length $\xi \sim \lambda^2$. Full horizontal mixing is attained once $\xi \sim N$. This implies a border $\tilde{\lambda}_{\rm mix} \sim \sqrt{N}$ at which "horizontal ergodicity" $\overline{\Delta x_\nu}/\Delta x_{\rm shl} \approx 1$ is attained.

C. The Wigner regime

Once the horizontal mixing is achieved, we get into the Wigner regime of vertical spreading, where the WBRM theory applies. A terse summary of the WBRM theory is provided in Appendix A. The mixed levels form a core of vertical width $\Gamma_E \propto \lambda^2$. This core determines the participation number $\mathcal{M}_\nu$. Full ergodicity is reached once Γ_E becomes comparable with the vertical width of the energy shell [Eq. (11)]. Consequently, the expected ergodicity threshold is $\tilde{\lambda}_{\rm erg} \sim \sqrt{b}$.

D. The ergodic regime

For $\lambda > \lambda_{\rm erg}$, there is full mixing within the energy shell, both horizontally and vertically. This regime is semiclassical. To the extent it conforms to the WBRM model, we can say that in the Wigner regime $\Gamma_E \ll \Delta_E < \Delta_b$, while in the ergodic regime $\Gamma_E \sim \Delta_E > \Delta_b$, where Γ_E indicates the width of the "core" region of nonperturbative mixing.

E. The integrable regime

Finally, when $\lambda \gg K$, the intrasystem hopping may be neglected and the system is reduced to the sum of disconnected integrable Bose-Hubbard dimers. Consequently, ergodicity is lost, M_ν and $\Delta\varepsilon_\nu$ decrease, and the state-to-state variance σ_x increases as the ETH is violated. This regime is nonuniversal. In the WBRM, the somewhat analogous regime is the Anderson regime $\tilde{\lambda} > b^{3/2}$ (see Appendix A for details).

IX. FALSE ERGODICITY MEASURES

Unlike $\overline{\mathcal{M}_\nu}/\mathcal{M}_{\rm shl}$, the ratio $\overline{\Delta\varepsilon_\nu}/\Delta\varepsilon_{\rm shl}$ cannot be used as an ergodicity measure. In fact, the first equality in Eq. (11) implies that the latter ratio is of order unity, irrespective of ergodicity. As discussed in Sec. IV B, a straightforward argument shows that $\Delta\varepsilon_\nu$ for any eigenstate is determined by the strength of the perturbation V, and is linear in λ. This is true even if the eigenstate is localized within the energy shell. The most dramatic demonstration is based on Eq. (20) for which $\mathcal{M} \sim 1$, but nevertheless the dispersion $\Delta\varepsilon_\nu$ is determined by the tails, and is not affected by $\mathcal{M}$. Consequently, the linear λ dependence of $\overline{\Delta\varepsilon_\nu}$ is *insensitive* to both the $\tilde{\lambda}_{\rm mix}$ and the $\tilde{\lambda}_{\rm erg}$ thresholds; hence, it cannot be used as an ergodicity measure.

X. THE REGIME BORDERS

Consider the scaling of the mixing and ergodicity borders $\lambda_{\rm mix}$ and the $\lambda_{\rm erg}$, with N. Within a semiclassical treatment, a rough estimate for the localization length is $\xi = (1/\Delta_0)D_x$, where the diffusion coefficient in x is $D_x = N^2 D_{cl}(\lambda)$. Note that $D_{cl} \propto [\lambda V_{cl}]^2$, where V_{cl} is the strength of perturbation in "classical" units. The density of states is $(1/\Delta_0) = N^d \Omega_{cl}$, where the number of degrees of freedom is $d = M-1$, and Ω_{cl} is the phase-space area of the energy shell. We note that ξ is possibly larger as discussed in Ref. [30]. From $\xi < N$, we get the condition

$$\Omega_{cl} D_{cl}(\lambda) < (1/N)^{1+d} \quad \rightsquigarrow \lambda_{\rm mix}. \tag{21}$$

Turning to the ergodic border, the condition is $\Gamma_E < \Delta_b$. The Feingold-Peres relation [3–6] (equivalent to ETH) is Eq. (6) of Ref. [15] that relates matrix elements to fluctuations. It is implied that $\Delta_b = \hbar/\tau_{cl}$, and that $\Gamma_E = (1/\Delta_0)\lambda^2 \bar{V}^2 = \lambda^2 V_{cl}^2 \tau_{cl}/\hbar$. Here, $\hbar = 1/N$. Thus, we get the condition

$$\lambda^2 V_{cl}^2 \tau_{cl}^2 < (1/N)^2 \rightsquigarrow \lambda_{\rm erg}. \tag{22}$$

Comparing the two conditions, we conclude that for large N, the mixing border is typically encountered before the ergodic border.

XI. SUMMARY

There are numerous studies where thermalization of one-dimensional spin chains is considered [17–20]. The perturbation λV in such models is responsible for nonintegrability, and the length L comes into consideration within a framework of a finite-size scaling scheme. The paradigm that we use for thermalization is quite different. It is motivated by the realization that thermalization of large disordered system can be modeled as the ergodization of small nearby chaotic subsystems that exchange particles and energy, sometimes referred to as hot spots [37].

No special assumptions about the subsystem geometry are made in our model, and L is not a physically meaningful geometrical parameter for the analysis. The number of sites $M_{\text{subsystem}}$ should be larger than 2 in order to have chaos, or better larger than 3 in order to avoid Kolmogorov-Arnold-Moser phase-space barriers (we used $M_A = M_B = 4$). The spectral structure illustrated in Fig. 1(b) as well as the distinction between horizontal and vertical ergodization demonstrated in Fig. 4 are not system specific and apply to all bipartite composite systems, regardless of their geometry or size. This point is further demonstrated in Appendix B. What really counts is the Hilbert space dimension, and hence the number of particles (N) has appeared in our discussion.

RMT modeling provides a partial understanding of the *route* toward ergodization. For physical subsytems, a more careful definition of the energy-shell concept is required. Then, it becomes clear that two distinct steps are involved, with different thresholds λ_{mix} and λ_{erg}, that signify spectral quantum chaos and ETH ergodization, respectively.

ACKNOWLEDGMENTS

A.V. acknowledges support from the NSF through a grant for ITAMP at Harvard University. D.C. acknowledges support by the Israel Science Foundation, Grant No. 518/22.

DATA AVAILABILITY

The data that support the findings of this article are not publicly available. The data are available from the authors upon reasonable request.

APPENDIX A: THE WBRM MODEL

The WBRM can be written schematically as follows:

$$H = \text{diag}\{\varepsilon_n\} + \text{offdiag}\{W_{n,m}\}. \tag{A1}$$

Parameters:

$$\Delta_0 = \text{level spacing}, \tag{A2}$$

$$\Delta_b = \text{range of hopping}, \tag{A3}$$

$$\bar{W} = \text{strength of hopping}. \tag{A4}$$

Dimensionless parameters

$$b = \frac{\Delta_b}{\Delta_0} = \text{dimensionless band width}, \tag{A5}$$

$$\lambda = \frac{\bar{W}}{\Delta_0} = \text{dimensionless coupling}. \tag{A6}$$

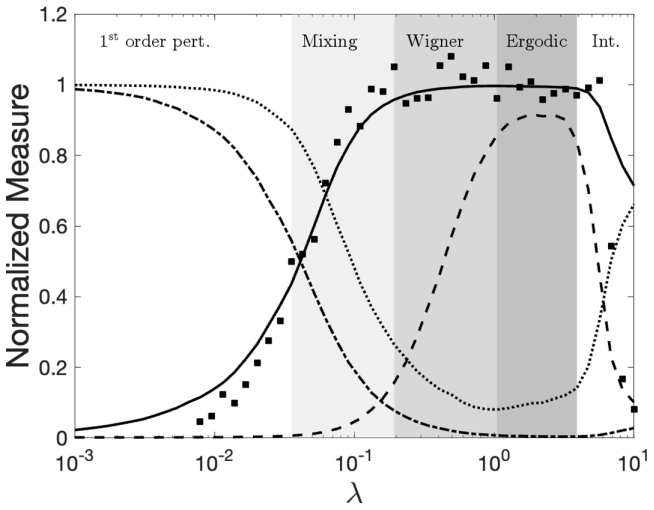


FIG. 5. Chaos and ergodicity measures. Same as Fig. 3 but with random internal couplings between all the sites of the coupled subsystems, selected from a normal distribution with zero mean and unit standard deviation. Thus, each subsystem is not a chain, but a fully connected cluster of arbitrary geometry.

The Wigner regime is

$$1 < \lambda < \sqrt{b}. \tag{A7}$$

In this regime, there are two "width" scales. One is Γ_E defined via PN calculation, and the other is Δ_E defined via a second moment calculation. One obtains

$$\Gamma_E = 2\pi \frac{\bar{W}^2}{\Delta_0}, \tag{A8}$$

$$\Delta_E = \sqrt{b}\bar{W}. \tag{A9}$$

Accordingly,

$$\frac{\Gamma_E}{\Delta_0} = 2\pi\lambda^2 = \text{dimensionless core width}, \tag{A10}$$

$$\frac{\Delta_E}{\Delta_0} = \sqrt{b}\lambda = \text{dimensionless shell width}. \tag{A11}$$

In the nonergodic Wigner regime $\Gamma_E \ll \Delta_E < \Delta_b$, while in the ergodic regime $\Gamma_E \sim \Delta_E > \Delta_b$. Note that in the RMT model, there is also an Anderson localization regime $\lambda > b^{3/2}$, where the Γ_E/Δ_0 width saturates to the value $\Delta_\xi/\Delta_0 = \xi \sim b^2$, that is much smaller than the unbounded semiclassically expected result $\Delta_E/\Delta_0 \propto \lambda$.

APPENDIX B: IRRELEVANCE OF GEOMETRY

In order to demonstrate the irrelevance of geometry in the context of our analysis, we have generated numerical results for coupled subsystems, where each subsystem is a fully connected cluster rather than a chain. The results are presented in Fig. 5. All the main features of Fig. 3 and, in particular, all five coupling regimes remain unchanged.

[1] E. P. Wigner, Characteristic vectors of bordered matrices with infinite dimensions, Ann. Math. **62**, 548 (1955); Characteristics vectors of bordered matrices with infinite dimensions II, **65**, 203 (1957).

[2] D. Cohen, F. M. Izrailev, and T. Kottos, Wavepacket dynamics in energy space, RMT and quantum-classical correspondence, Phys. Rev. Lett. **84**, 2052 (2000).

[3] M. Feingold and A. Peres, Distribution of matrix elements of chaotic systems, Phys. Rev. A **34**, 591 (1986).

[4] M. Feingold, D. Leitner, and M. Wilkinson, Spectral statistics in semiclassical random-matrix ensembles, Phys. Rev. Lett. **66**, 986 (1991).

[5] M. Wilkinson, M. Feingold, and D. Leitner, Localization and spectral statistics in a banded random matrix ensemble, J. Phys. A **24**, 175 (1991).

[6] M. Feingold, A. Gioletta, F. M. Izrailev, and L. Molinari, Two-parameter scaling in the Wigner ensemble, Phys. Rev. Lett. **70**, 2936 (1993).

[7] V. V. Flambaum, A. A. Gribakina, G. F. Gribakin, and M. G. Kozlov, Structure of compound states in the chaotic spectrum of the Ce atom: Localization properties, matrix elements, and enhancement of weak perturbations, Phys. Rev. A **50**, 267 (1994).

[8] G. Casati, B. V. Chirikov, I. Guarneri, and F. M. Izrailev, Band-random-matrix model for quantum localization in conservative systems, Phys. Rev. E **48**, R1613 (1993).

[9] G. Casati, B. V. Chirikov, I. Guarneri, and F. M. Izrailev, Quantum ergodicity and localization in conservative systems: The Wigner band random matrix model, Phys. Lett. A **223**, 430 (1996).

[10] M. V. Berry, Regular and irregular semiclassical wavefunctions, J. Phys. A **10**, 2083 (1977).

[11] J. M. Deutsch, Quantum statistical mechanics in a closed system, Phys. Rev. A **43**, 2046 (1991).

[12] M. Srednicki, Chaos and quantum thermalization, Phys. Rev. E **50**, 888 (1994).

[13] F. Borgonovi, I. Guarneri, and F. M. Izrailev, Quantum-classical correspondence in energy space: Two interacting spin particles, Phys. Rev. E **57**, 5291 (1998).

[14] D. Cohen and E. J. Heller, Unification of perturbation theory, RMT and semiclassical considerations in the study of parametrically-dependent eigenstates, Phys. Rev. Lett. **84**, 2841 (2000).

[15] D. Cohen and T. Kottos, Parametric dependent hamiltonians, wavefunctions, random-matrix-theory, and quantal-classical correspondence, Phys. Rev. E **63**, 036203 (2001).

[16] M. Rigol, V. Dunjko, and M. Olshanii, Thermalization and its mechanism for generic isolated quantum systems, Nature (London) **452**, 854 (2008).

[17] D. A. Rabson, B. N. Narozhny, and A. J. Millis, Crossover from Poisson to Wigner-Dyson level statistics in spin chains with integrability breaking, Phys. Rev. B **69**, 054403 (2004).

[18] L. F. Santos and M. Rigol, Onset of quantum chaos in one-dimensional bosonic and fermionic systems and its relation to thermalization, Phys. Rev. E **81**, 036206 (2010).

[19] L. F. Santos and M. Rigol, Localization and the effects of symmetries in the thermalization properties of one-dimensional quantum systems, Phys. Rev. E **82**, 031130 (2013).

[20] M. Rigol, Fundamental asymmetry in quenches between integrable and nonintegrable systems, Phys. Rev. Lett. **116**, 100601 (2016).

[21] M. Pandey, P. W. Claeys, D. K. Campbell, A. Polkovnikov, and D. Sels, Adiabatic eigenstate deformations as a sensitive probe for quantum chaos, Phys. Rev. X **10**, 041017 (2020).

[22] T. LeBlond, D. Sels, A. Polkovnikov, and M. Rigol, Universality in the onset of quantum chaos in many-body systems, Phys. Rev. B **104**, L201117 (2021).

[23] J. J. Pulikkottil, A. Lakshminarayan, S. C. L. Srivastava, M. F. I. Kieler, A. Backer, and S. Tomsovic, Quantum coherence controls the nature of equilibration and thermalization in coupled chaotic systems, Phys. Rev. E **107**, 024124 (2023).

[24] H. Gersch and G. Knollman, Quantum cell model for bosons, Phys. Rev. **129**, 959 (1963).

[25] D. Jaksch, C. Bruder, J. Cirac, C. Gardiner, and P. Zoller, Cold bosonic atoms in optical lattices, Phys. Rev. Lett. **81**, 3108 (1998).

[26] D. Jaksch and P. Zoller, The cold atom Hubbard toolbox, Ann. Phys. **315**, 52 (2005).

[27] F. H. L. Essler, H. Frahm, F. Göhmann, A. Klümper, and V. E. Korepin, *The One-Dimensional Hubbard Model* (Cambridge University Press, Cambridge, UK, 2005).

[28] A. V. Ponomarev, S. Denisov, and P. Hänggi, Thermal equilibration between two quantum systems, Phys. Rev. Lett. **106**, 010405 (2011).

[29] I. Tikhonenkov, A. Vardi, J. R. Anglin, and D. Cohen, Minimal Fokker-Planck theory for the thermalization of mesoscopic subsystems, Phys. Rev. Lett. **110**, 050401 (2013).

[30] C. Khripkov, A. Vardi, and D. Cohen, Semiclassical theory of strong localization for quantum thermalization, Phys. Rev. E **97**, 022127 (2018).

[31] C. Khripkov, A. Vardi, and D. Cohen, Many body dynamical localization and thermalization, Phys. Rev. A **101**, 043603 (2020).

[32] Y. Y. Atas, E. Bogomolny, O. Giraud, and G. Roux, Distribution of the ratio of consecutive level spacings in random matrix ensembles, Phys. Rev. Lett. **110**, 084101 (2013).

[33] V. A. Yurovsky and M. Olshanii, Memory of the initial conditions in an incompletely chaotic quantum system universal predictions with application to cold atoms, Phys. Rev. Lett. **106**, 025303 (2011).

[34] V. A. Yurovsky, Exploring integrability-chaos transition with a sequence of independent perturbations, Phys. Rev. Lett. **130**, 020404 (2023).

[35] V. A. Yurovsky, Quantum chaos in a harmonic waveguide with scatterers, SciPost Phys. **15**, 221 (2023).

[36] V. A. Yurovsky and A. Vardi, Eigenstate thermalization to non-monotonic distributions in strongly-interacting chaotic lattice gases, arXiv:2501.08967.

[37] D. M. Basko, Weak chaos in the disordered nonlinear Schrodinger chain: Destruction of Anderson localization by Arnold diffusion, Ann. Phys. **326**, 1577 (2011).

Correction: A misprint in the heading for Sec. V has been fixed.